Available online at www.sciencedirect.com
SCIENCE DIRECT®
Journal of Computational Physics 195 (2004) 594–601
JOURNAL OF COMPUTATIONAL PHYSICS
www.elsevier.com/locate/jcp

A high-wavenumber viscosity for high-resolution numerical methods

Andrew W. Cook *, William H. Cabot

Lawrence Livermore National Laboratory, P.O. Box 808, Livermore, CA 94551, USA

Received 4 March 2003; received in revised form 5 August 2003; accepted 9 October 2003

Abstract

A spectral-like viscosity is proposed for centered differencing schemes to help stabilize numerical solutions and reduce oscillations near discontinuities. Errors introduced by the added dissipation can be made arbitrarily small by adjusting the power of the derivative in the viscosity term. The high-wavenumber viscosity is combined with a 10th-order compact scheme to produce an accurate and efficient shock-capturing method. The new scheme compares favorably with other shock-capturing algorithms.

PACS: 47.11.+j

Keywords: Artificial viscosity; Compact schemes; Shock capturing

For flows with a wide range of scales, global differencing schemes, e.g., spectral and compact methods, have far greater resolving power than local schemes, e.g., explicit finite-difference methods [1–3]. The desire for accurate simulations of flows involving both discontinuities and a broad spectrum, e.g., shock-turbulence interactions, has driven recent work in extending global schemes to accommodate shocks. Deng et al. [4,5] introduced compact stencils and interpolants into the ENO/WENO framework in an effort to improve the modified wavenumber compared to explicit upwinding. Yee et al. [6] and Gaitonde and Visbal [7] employed characteristic-based and Padé-type filters to smooth the solution near shocks and stabilize their calculations. In this note, we explore the merits of adding a wavenumber-weighted viscosity to control Gibbs oscillations near shocks. The idea of adding artificial dissipation terms to central schemes to capture discontinuities is an old one, originating with von Neumann and Richtmyer [8] half a century ago. Jameson et al. [9] added 2nd- and 4th-order dissipation terms to regularize numerical solutions to the Euler equations. The historical drawback of the artificial viscosity approach is that the added terms are frequently too dissipative in certain regions of the flow. To minimize undesirable dissipation Tadmor [10] developed a spectral vanishing viscosity (SVV) approach, which has been demonstrated by Karamanos and Karniadakis [11] to provide good

* Corresponding author. Tel.: +1-423-2856; fax: +1-423-0925.
E-mail address: awcook@llnl.gov (A.W. Cook).

0021-9991/$ - see front matter
doi:10.1016/j.jcp.2003.10.012

control of the small scales in large-eddy simulations of high Reynolds number flows. Here we explore an idea for simulating compressible flows, similar to the SVV approach, but with three differences: first, the dissipation is applied in physical space; second, the viscosity kernel uses information directly from the resolved scales; and third, the added term takes the form of the Navier–Stokes viscous stress, such that the method converges to a DNS with sufficient refinement.

In one dimension, the Euler equations for inviscid flow of an ideal gas are:

$$\frac{\partial \rho}{\partial t} + \frac{\partial \rho u}{\partial x} = 0, \tag{1}$$

$$\frac{\partial \rho u}{\partial t} + \frac{\partial}{\partial x}(\rho uu + p) = 0, \tag{2}$$

$$\frac{\partial \rho E}{\partial t} + \frac{\partial}{\partial x}[(\rho E + p)u] = 0, \tag{3}$$

$$p = (\gamma - 1)\rho e, \tag{4}$$

where ρ is density, u is velocity, p is pressure, $E = (e + uu/2)$ is total energy, e is internal energy and γ is the ratio of specific heats. This system can be regularized by replacing (2) and (3) with

$$\frac{\partial \rho u}{\partial t} + \frac{\partial}{\partial x}(\rho uu + p - \tau) = 0 \tag{5}$$

and

$$\frac{\partial \rho E}{\partial t} + \frac{\partial}{\partial x}[(\rho E + p - \tau)u] = 0, \tag{6}$$

where

$$\tau = \mu \frac{\partial u}{\partial x} \tag{7}$$

is a viscous stress and μ is a grid-dependent artificial viscosity. A "high resolution" numerical method is a scheme in which τ only damps wavenumbers close to the Nyquist wavenumber, $\pi/\Delta x$. This can be accomplished by making $\mu \propto \partial^r u/\partial x^r$, where r is a user-specified integer, thus imparting to μ a high wavenumber (k^r) bias. This type of artificial selective damping has been successfully employed in acoustics computations by Tam et al. [12], and by Barone and Lele [13] who set $\tau \propto \partial^r u/\partial x^r$. In our formulation, we base μ, rather than τ, on the r-derivative in order to make (5) assume Navier–Stokes form.

Now consider a periodic isentropic flow, where (1)–(3) can each be cast in the form

$$\frac{\partial \phi}{\partial t} + \theta \frac{\partial \phi}{\partial x} = 0, \tag{8}$$

where θ is a wave speed and ϕ is a Riemann invariant [14]. For the purpose of analysis, θ will be taken as constant. The spatially-discrete analogue of (8) is

$$\frac{\partial \phi_j}{\partial t} + \theta D \cdot \phi_j = 0, \tag{9}$$

where j is a grid index and $D\cdot$ denotes a discrete operator approximating $\partial/\partial x$. Fourier transforms ($\mathscr{F}$) of (8) and (9) can be written as

$$\frac{\partial\phi(k)}{\partial t} + \theta(\mathrm{i}k/\Delta x)\phi(k) = 0 \tag{10}$$

and

$$\frac{\partial\phi_k}{\partial t} + \theta(\mathrm{i}\omega/\Delta x)\phi_k = 0, \tag{11}$$

respectively, where $\phi(k) = \mathscr{F}\{\phi(x)\}$, $\phi_k = \mathscr{F}\{\phi_j\}$, k is a nondimensional wavenumber (ranging from 0 to π) and $\omega = \omega(k)$ is a nondimensional modified wavenumber. The modified wavenumber for spatial discretization of the form

$$\beta\phi'_{j-2} + \alpha\phi'_{j-1} + \phi'_j + \alpha\phi'_{j+1} + \beta\phi'_{j+2} = c\frac{\phi_{j+3} - \phi_{j-3}}{6\Delta x} + b\frac{\phi_{j+2} - \phi_{j-2}}{4\Delta x} + a\frac{\phi_{j+1} - \phi_{j-1}}{2\Delta x} \tag{12}$$

is [2,3]

$$\omega(k) = \frac{a\sin(k) + (b/2)\sin(2k) + (c/3)\sin(3k)}{1 + 2\alpha\cos(k) + 2\beta\cos(2k)}. \tag{13}$$

In this note, we consider a 4th-order explicit (E4) scheme ($\alpha = 0,\ \beta = 0,\ a = 4/3,\ b = -1/3,\ c = 0$), a 4th-order compact (C4) scheme ($\alpha = 1/4,\ \beta = 0,\ a = 3/2,\ b = 0,\ c = 0$), a 10th-order compact (C10) scheme ($\alpha = 1/2,\ \beta = 1/20,\ a = 17/12,\ b = 101/150,\ c = 1/100$), and a spectral (S) Fourier transform scheme for which $\omega = k$.

The spatial discretization is combined with a five-step 4th-order Runge–Kutta (RK4) method derived by Kennedy et al. [15]. For differential equations of the form $\dot{\phi} = f$, the scheme is

$$q^\eta = \Delta t f^{\eta-1} + A^\eta q^{\eta-1}, \quad \phi^\eta = \phi^{\eta-1} + B^\eta q^\eta, \qquad \eta = 1,\ldots,5, \tag{14}$$

where Δt is the time step, η is the RK4 subcycle, and A^η and B^η are: $A^1 = 0,\ A^2 = -6234157559845/12983515589748,\ A^3 = -6194124222391/4410992767914,\ A^4 = -31623096876824/15682348800105,\ A^5 = -12251185447671/11596622555746,\ B^1 = 494393426753/4806282396855,\ B^2 = 4047970641027/5463924506627,\ B^3 = 9795748752853/13190207949281,\ B^4 = 4009051133189/8539092990294,\ B^5 = 1348533437543/7166442652324$. This particular RK4 scheme was chosen for its broad stability properties for both convective and viscous terms. The amplification factor is

$$A_\mathrm{N} = \frac{\phi_k^{\eta=5}}{\phi_k^{\eta=0}} = \left[1 - \frac{\psi_\omega^2}{2} + \frac{\psi_\omega^4}{24}\right] - \mathrm{i}\left[\psi_\omega - \frac{\psi_\omega^3}{6} + \frac{\psi_\omega^5}{200}\right], \tag{15}$$

where $\psi_\omega \equiv \omega\Theta$ and $\Theta \equiv \theta\Delta t/\Delta x$ is the CFL number. Maximum stable CFL numbers ($|A_\mathrm{N}| = 1$) for the E4-RK4, C4-RK4, C10-RK4 and S-RK4 schemes are 2.435, 1.929, 1.437 and 1.063, respectively.

The exact solution to (10) at $t = n\Delta t$ is $\phi^n(k) = \Phi\exp(-\mathrm{i}kn\Theta)$ with amplification factor

$$A_\mathrm{E} \equiv \frac{\phi^{n+1}(k)}{\phi^n(k)} = \exp(-\mathrm{i}\psi_k) = \left[1 - \frac{\psi_k^2}{2} + \frac{\psi_k^4}{24} - \frac{\psi_k^6}{720} + \mathscr{O}(\psi_k^8)\right] - \mathrm{i}\left[\psi_k - \frac{\psi_k^3}{6} + \frac{\psi_k^5}{120} - \mathscr{O}(\psi_k^7)\right], \tag{16}$$

where $\psi_k \equiv k\Theta$. The total error (spatial plus temporal) for the centered-space Runge–Kutta schemes is $\mathscr{E}_\mathrm{N} = A_\mathrm{N} - A_\mathrm{E}$. The real part of $\mathscr{E}_\mathrm{N}$ is the diffusive error and the imaginary part is the dispersive error. The errors increase at higher wavenumbers and higher CFL numbers. Therefore, the optimum CFL number depends on the spectral content of the flow, and hence will vary depending on the problem.

To see how a wavenumber-weighted viscosity affects the overall error, add a term of the form $\nu k^r\phi(k)/\Delta x^2$ to the right-hand side of Eq. (10). The amplification factor for the exact solution with artificial

viscosity is $A_V = \exp(\sigma k^r - ik\Theta)$, where ν is a kinematic viscosity parameter and $\sigma \equiv \nu\Delta t/\Delta x^2$. The error introduced by the spectral-like viscosity is

$$\mathscr{E}_V = A_V - A_E = \exp(\sigma k^r - ik\Theta) - \exp(-ik\Theta) = \left[\sigma k^r + \mathscr{O}\left(k^{2r}\right)\right] - i\left[\sigma k^{r+1} + \mathscr{O}\left(k^{2r+1}\right)\right]. \tag{17}$$

For small k, we can choose r sufficiently large that $\mathscr{E}_V < \mathscr{E}_N$; i.e., we can ensure that the error introduced by the artificial viscosity is less than the space–time discretization errors already present.

The particular form of artificial viscosity employed in our simulations is

$$\mu = C_\mu \rho (\Delta x)^{r+1} \overline{\left|\frac{\partial^r u}{\partial x^r}\right|}, \tag{18}$$

where $\overline{|\ |}$ denotes a Gaussian filter applied to the absolute value to ensure that μ is smooth and positive. It is desirable to choose r as large as possible to minimize the error caused by introducing τ into the equations. However, larger values of r require larger stencils to accurately represent the r-derivative. Compact (Padé) schemes provide a means whereby high derivatives can be computed with reasonably small stencils. For the current simulations we chose $r = 8$ and used the 6th-order approximation (which was found to be the minimum order necessary to achieve the desired results),

$$\begin{aligned} &29u_j^{VIII} + 14\left(u_{j+1}^{VIII} + u_{j-1}^{VIII}\right) + (3/2)\left(u_{j+2}^{VIII} + u_{j-2}^{VIII}\right) \\ &\quad = [4200u_j - 3360(u_{j+1} + u_{j-1}) + 1680(u_{j+2} + u_{j-2}) \\ &\qquad - 480(u_{j+3} + u_{j-3}) + 60(u_{j+4} + u_{j-4})]/(\Delta x)^8, \end{aligned} \tag{19}$$

where u_j^{VIII} approximates $\partial^8 u/\partial x^8$ at the jth grid point. The filter is then applied as

$$\begin{aligned} \overline{\left|u_j^{VIII}\right|} = {} & \frac{3565}{10368}\left|u_j^{VIII}\right| + \frac{3091}{12960}\left(\left|u_{j+1}^{VIII}\right| + \left|u_{j-1}^{VIII}\right|\right) + \frac{1997}{25920}\left(\left|u_{j+2}^{VIII}\right| + \left|u_{j-2}^{VIII}\right|\right) \\ & + \frac{149}{12960}\left(\left|u_{j+3}^{VIII}\right| + \left|u_{j-3}^{VIII}\right|\right) + \frac{107}{103680}\left(\left|u_{j+4}^{VIII}\right| + \left|u_{j-4}^{VIII}\right|\right), \end{aligned} \tag{20}$$

which is derived by matching the transfer function to a Gaussian of width $4\Delta x$. For the calculations presented here, $C_\mu = 0.1$. The C10-RK4 scheme with artificial terms is denoted C10V-RK4.

Our test problem is a compressible breaking wave with initial conditions

$$\rho/\rho_0 = 1 + \epsilon \sin(2\pi x/\lambda), \tag{21}$$

$$p/p_0 = (\rho/\rho_0)^\gamma, \tag{22}$$

$$c_s/c_{s0} = (\rho/\rho_0)^{(\gamma-1)/2}, \tag{23}$$

$$u = 2(c_{s0} - c_s)/(\gamma - 1), \tag{24}$$

where c_s is the sound speed, $\rho_0 = 10^{-3}$, $p_0 = 10^6$, $\gamma = 5/3$ and $\epsilon = 0.1$. The wavelength, λ, is set to $N\Delta x$, where N is the number of grid points per period. For this set of initial conditions, two of the three characteristics are initially constant, with the third satisfying a Burgers-like equation. The exact solution consists of the initial profiles being advected with velocity $u - c_s$, hence points on the profiles move from x to $\xi = x + (u - c_s)t$. A discontinuity begins to form when the solution attempts to become multivalued; this happens for a given x at

$$t = \frac{\lambda}{(\gamma+1)\pi\epsilon c_{s0}} \frac{[1 + \epsilon \sin(2\pi x/\lambda)]^{(3-\gamma)/2}}{\cos(2\pi x/\lambda)}, \tag{25}$$

which has the minimum

$$\sin(2\pi x_b/\lambda) = -\frac{1}{(\gamma-1)\epsilon} + \left(\frac{1}{(\gamma-1)^2\epsilon^2} - \frac{3-\gamma}{\gamma-1}\right)^{1/2}. \tag{26}$$

For $\epsilon \ll 1$, $\sin(2\pi x_b/\lambda) \approx -(3-\gamma)\epsilon/2$ and $t_b = [\lambda/(\gamma+1)\pi\epsilon c_{s0}][1+O(\epsilon^3)]$, where t_b denotes the time when the wave first begins to break. The discontinuity therefore forms very near the point initially corresponding to $x = 0$ and grows to include more points on either side. The peaks of the initial sinusoidal profile at $x_p = \pm\lambda/4$ reach this point at a later time given by

$$t_p \approx \frac{(\gamma-1)(x_b - x_p)}{(\gamma+1)(c_{s,b} - c_{s,p})} \approx \lambda/2(\gamma+1)\epsilon c_{s0} \approx (\pi/2)t_b. \tag{27}$$

At this time, the discontinuity reaches its greatest amplitude, after which it slowly decreases [14]. The analytical solution to this breaking wave is only valid for $t \leqslant t_b$ because, unlike pure Burgers flow, the shock processes fluid; hence, the entropy ceases to be constant for $t > t_b$.

Convergence rates for the centered RK4 schemes at $t = 3t_b/4$, when the flow is still smooth, are plotted in Fig. 1. At high CFL numbers, time-stepping errors determine the rates of convergence; however, the actual errors are much lower for the higher-resolution spatial discretizations. For instance, errors for the C10-RK4 scheme are more than an order of magnitude lower than those of the E4-RK4 scheme, even though both methods are formally 4th-order accurate at CFL = 1. At low CFL numbers, spatial discretization errors determine the rates of convergence; e.g., the C10-RK4 scheme exhibits 10th-order convergence at CFL = 1/16. When artificial viscosity is added to this scheme, the convergence rate is limited by the r parameter, which in this case gives 8th-order convergence. Note that 8th-order convergence is obtained even though the approximation to the 8th derivative is only 6th order.

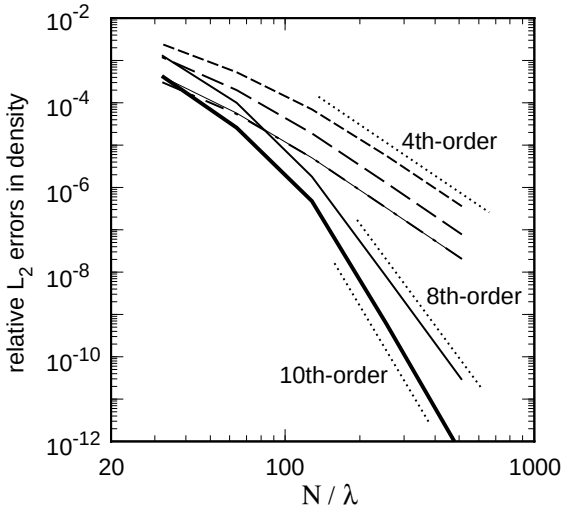

Fig. 1. Convergence rates for the centered RK4 schemes at $t = 3t_b/4$: C10-RK4 at CFL = 1/16 (heavy solid), C10V-RK4 at CFL = 1/16 (medium solid), C10-RK4 at CFL = 1 (thin solid) nearly coincident with S-RK4 at CFL = 1 (dot-dashed), C4-RK4 at CFL = 1 (long dashed), E4-RK4 at CFL = 1 (short dashed). Fiducial lines corresponding to 4th-, 8th-, and 10th-order convergence are also plotted for reference.

Next, we compare the accuracy of the C10V-RK4 method against two standard shock-capturing methods, which have been published extensively in the literature: Jiang and Shu's 5th-order Weighted Essentially Non-Oscillatory method with 3rd-order TVD Runge–Kutta time-stepping (WENO5-RK3) [16], and Bell and Colella's 2nd-order Piecewise Linear MUSCL Direct Eulerian (PLMDE) method [17,18]. Errors for the C10V-RK4, WENO5-RK3 and PLMDE methods are plotted versus time in Fig. 2 for CFL = 1 and $N/\lambda = 128$. During the smooth phase, the error for the C10V-RK4 scheme is a couple orders of magnitude lower than the WENO5-RK3 error, which, in turn, is about an order of magnitude lower than the PLMDE error. However, as the discontinuity forms, the errors for all three schemes become similar, and the rates of convergence all become first order. A scale-dependent measure of error is given in Fig. 3, which displays the density energy spectrum for the shock-capturing schemes at $t = 3t_b/4$ with $N/\lambda = 64$. The spectra provide a direct measure of the resolving power of each scheme. Two facts are evident from the plot; first, the C10-RK4 and C10V-RK4 methods have nearly identical resolution properties, which means that the high-wavenumber viscosity has negligible impact on the solution in smooth regions; and second, the C10 schemes give excellent representation for about half the wavenumbers, whereas the WENO5 and PLMDE schemes match less than a quarter of the wavenumbers. This is a consequence of the fact that the C10 schemes are purely centered, whereas the WENO5 and PLMDE methods are upwinded. The modified wavenumber for centered schemes is real (as is the true wavenumber), whereas the modified wavenumber for non-centered schemes is complex.

The efficiency of the schemes is quantified in Table 1, which displays the CPU time required for each scheme to reach $t/t_b = 3/4$ (with CFL = 1), at the resolution necessary to meet the indicated L_2 error. By this measure, the centered schemes are vastly more efficient than the upwinded methods because they are able to satisfy the error tolerance with much fewer grid points.

The picture changes, however, when the flow becomes discontinuous. Fig. 4 displays the density solution for the C10V-RK4, WENO5-RK3 and PLMDE methods at $t = t_p$, the time at which the discontinuity reaches its greatest amplitude. For this time, the 'exact' solution is taken as the PLMDE result with $N/\lambda = 20{,}000$. For all three schemes, the shock is spread over about four grid points and oscillations are negligible. Results for the C10-RK4 scheme (without artificial viscosity) exhibit strong Gibbs oscillations

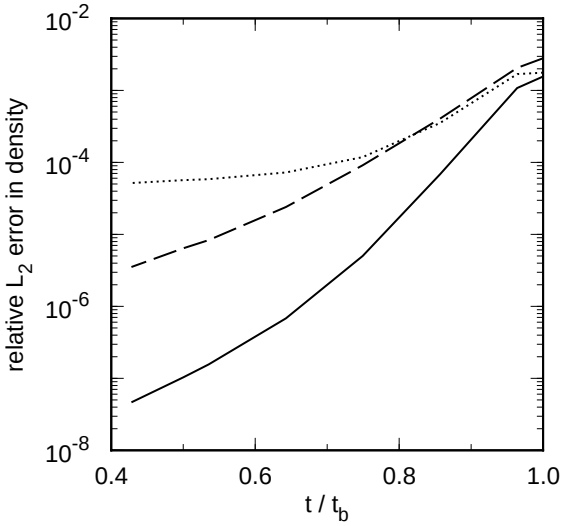

Fig. 2. L_2 errors for C10V-RK4 (solid), WENO5-RK3 (dashed) and PLMDE (dotted) at CFL = 1 and $N/\lambda = 128$.

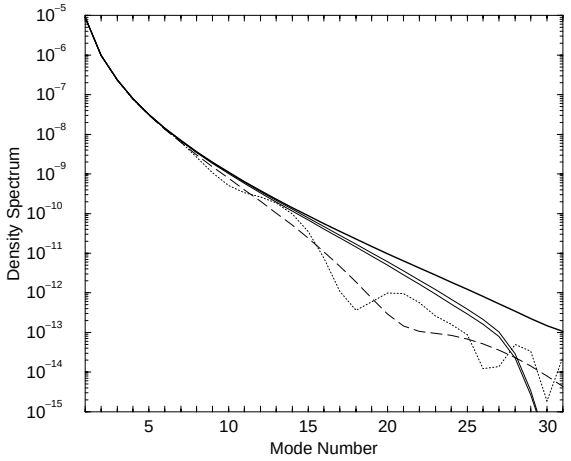

Fig. 3. Density spectrum at $t = 3t_b/4$ with $N/\lambda = 64$: exact solution (thick solid), C10-RK4 (medium solid), C10V-RK4 (thin solid), WENO5-RK3 (dashed line) and PLMDE (dotted). All numerical solutions are computed at CFL = 1.

Table 1
CPU times and resolutions required to reach $t/t_b = 3/4$, at CFL = 1, to within the specified L_2 error

Scheme	N/λ	Time steps	CPU time (s)	L_2 error
E4-RK4	995	1004	1.467	2.03×10^{-8}
C4-RK4	715	722	0.777	2.03×10^{-8}
C10-RK4	512	516	0.583	2.03×10^{-8}
S-RK4	512	516	0.874	2.03×10^{-8}
C10V-RK4	512	516	1.40	2.03×10^{-8}
WENO5-RK3	2110	2157	76.0	2.03×10^{-8}
PLMDE	9900	9990	263	2.03×10^{-8}

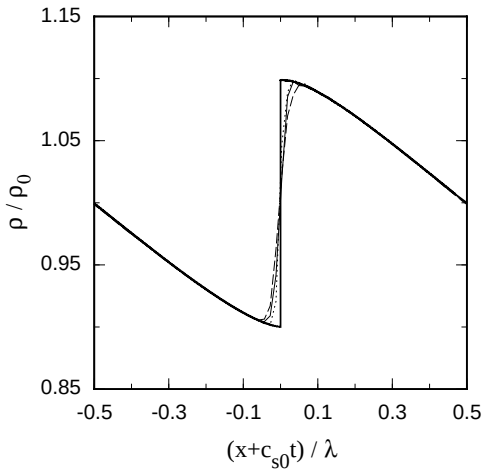

Fig. 4. Density computed with the PLMDE (dotted), WENO5-RK3 (dashed) and C10V-RK4 (thin solid) schemes at $t = t_p$ with $N/\lambda = 64$ using CFL = 1. The thick solid line is the PLMDE solution with $N/\lambda = 20{,}000$.

on both sides of the shock. The CPU times required for the C10V-RK4, WENO5-RK3 and PLMDE schemes to reach $t = t_p$ with $N/\lambda = 512$ and CFL = 1, were 2.91, 9.76 and 1.424 s, respectively.

In summary, we have proposed a spectral-like viscosity which can be added to any numerical method to reduce oscillations near discontinuities. We have demonstrated the convergence rates for smooth flow to be proportional to the power of the derivative in the artificial viscosity; hence, the error introduced by the added dissipation can be made arbitrarily small. We combined the high-wavenumber viscosity with the most efficient of the centered schemes tested to produce an accurate and efficient shock-capturing method (C10V-RK4). The new C10V-RK4 scheme was evaluated against standard shock-capturing schemes (WENO5-RK3 and PLMDE). For the smooth flow phase, the C10V-RK4 scheme proved much more efficient than either the WENO5-RK3 scheme or the PLMDE method, with differences increasing for lower error tolerances. For the discontinuous phase of the flow, errors for the shock-capturing schemes were similar, and C10V-RK4 proved several times more efficient than WENO5-RK3 and about half as efficient as PLMDE.

Acknowledgements

We thank Dr. W.J. Rider and Dr. J.A. Greenough for their assistance in obtaining the WENO and PLMDE results. This work was performed under the auspices of the US Department of Energy by the University of California Lawrence Livermore National Laboratory under contract No. W-7405-Eng-48.

References

[1] D. Gottlieb, S.A. Orszag, Numerical Analysis of Spectral Methods, Capital City Press, Montpelier, 1977.
[2] R. Vichnevetsky, J.B. Bowles, Fourier Analysis of Numerical Approximations of Hyperbolic Equations, SIAM, Philadelphia, 1982.
[3] S.K. Lele, Compact finite difference schemes with spectral like resolution, J. Comput. Phys. 103 (1992) 16–42.
[4] X. Deng, H. Maekawa, Compact high order accurate nonlinear schemes, J. Comput. Phys. 130 (1997) 77–91.
[5] X. Deng, H. Zhang, Developing high-order weighted compact nonlinear schemes, J. Comput. Phys. 165 (2000) 22–44.
[6] H.C. Yee, N.D. Sandham, M.J. Djomehri, Low-dissipative high-order shock-capturing methods using characteristic-based filters, J. Comput. Phys. 150 (1999) 199–238.
[7] D.V. Gaitonde, M.R. Visbal, Padé-type higher-order boundary filters for the Navier-Stokes equations, AIAA J. 38 (2000) 2103–2112.
[8] J. von Neumann, R.D. Richtmyer, A method for the numerical calculations of hydrodynamical shocks, J. Appl. Phys. 21(1950) 232.
[9] A. Jameson, W. Schmidt, E. Turkel, Numerical simulation of the Euler equations by finite volume methods using Runge-Kutta time stepping schemes, AIAA paper 81-1259, AIAA 5th Computations Fluid Dynamics Conference, 1981.
[10] E. Tadmor, Convergence of spectral methods for nonlinear conservation laws, SIAM J. Numer. Anal. 26 (1989) 30.
[11] G-S. Karamanos, G.E. Karniadakis, A spectral vanishing viscosity method for large-eddy simulations, J. Comput. Phys. 163 (2000) 22–50.
[12] C.K.W. Tam, J.W. Webb, Z. Dong, A study of the short wave components in computational aeroacoustics, J. Comput. Acoust. 1 (1993) 1–30.
[13] M.F. Barone, S.K. Lele, A numerical technique for trailing edge acoustic scattering problems, AIAA paper 2002-0226, 40th AIAA Aerospace Sciences Meeting and Exhibit, 2002.
[14] L.D. Landau, E.M. Lifshitz, Fluid Mechanics, Pergamon Press, 1959.
[15] C.A. Kennedy, M.H. Carpenter, R.M. Lewis, Low-storage, explicit Runge–Kutta schemes for the compressible Navier–Stokes equations, ICASE Report No. 99-22, 1999.
[16] G.-S. Jiang, C.-W. Shu, Efficient implementation of weighted ENO schemes, J. Comput. Phys. 126 (1996) 202–228.
[17] J.B. Bell, P. Colella, J. Trangenstein, Higher order Godunov methods for general systems of hyperbolic conservation laws, J. Comput. Phys. 82 (1989) 362–397.
[18] P. Colella, Multidimensional upwind methods for hyperbolic conservation laws, J. Comput. Phys. 87 (1990) 171–200.